Revealing the evolution of Cu^{II} species and ammonia intermediates under different temperatures for selective catalytic reduction of NO over cost-effective Cu-exchanged zeolite X catalysts

*Lin Chen [a, *], Yuanpei Lan [a, *], Chaoyi Chen [a], Shan Ren [b, *], Junqi Li [a], Davide Ferri [c]*

[a] School of Materials and Metallurgy, Guizhou University, Guizhou 550025, Guiyang, PR China

[b] School of Energy and Power Engineering, Xi'an Jiaotong University, Xi'an 710049, Shaanxi, PR China

[c] Paul Scherrer Institut, PSI Center for Energy and Environmental Sciences, CH-5232 Villigen PSI, Switzerland

* Corresponding authors' Emails: linchen@gzu.edu.cn, yplan@gzu.edu.cn，shanren@xjtu.edu.cn

Note: this file contains 24 pages, 4 tables and 16 figures.

Text S1 Characterization

Powder X-ray diffraction (XRD) data of calcined samples were acquired on a D8 Advance Bruker instrument equipped with a 1D-LynxEye detector using Cu Kα1 radiation (λ = 1.5406 Å) and at a step size of 0.02°, an acquisition time of 2 s, with 2q from 5° to 90°.

The transmission electron microscopy (TEM) morphology and elemental mapping of catalysts were measured on a JEOL JEM-F200 equipment with working at 200 kV.

The specific surface area (BET value), total pore volume, external surface area, micropore area, and volume (t-plot method, 0.2-0.5 P/P_0 range with the generalized Halsey model) were measured using an Autosorb iQ-XR (Anton Paar) equipped with a CryoSync accessory with Ar as the adsorbate using liquid N_2 at liquid Ar temperature (87 K). Prior to analysis, the samples were outgassed under high vacuum at 300 °C for 4 h.

Ultraviolet-visible spectra of the hydrated samples were recorded ex situ in diffuse reflectance mode (DRUV) under ambient conditions using a spectrometer (Varian Cary 4000) equipped with a Praying Mantis diffuse reflectance accessory (Harrick). $BaSO_4$ was used as reference material. Deconvolution of the Kubelka-Munk spectra in Gaussian bands was performed using the PeakFit 4.12 software.

Inductively coupled plasma optical emission spectrometer (ICP-OES) was used to calculated the Cu, Si and Al elements for the sample.

The ^{29}Si and ^{27}Al magic angle spinning nuclear magnetic resonance (MAS NMR) single pulse experiments were performed on a Bruker Avance III NMR spectrometer (Bruker Biospin AG, Switzerland) using a 4 mm cross polarization magic angle spinning (CP/MAS) probe at 13 MHz.

Temperature-programmed desorption of ammonia (NH_3-TPD) was carried out in a quartz glass reactor (6 mm inner diameter). The sample (0.05 g catalyst and 0.05 g cordierite,150 μm mesh) was loaded into the reactor within two quartz wool plugs and was treated in a N_2 flow (100 mL/min) at 300 °C for 60 min (10 °C /min). After cooling to 50 °C, NH_3 adsorption was carried out until saturation (500 ppm of NH_3/N_2, 100 mL/min), followed by N_2 purge to remove physisorbed NH_3. Desorption was carried out in 100 mL/min N_2 from 50 to 600 °C at 10 °C /min, and the concentration of NH_3 was measured online using an FTIR spectrometer (Antaris, Thermo Scientific) equipped with a heated transmission cell.

Text S2 Kinetic analysis

The NH_3-SCR kinetic parameter of NO_x conversion were calculated by using the NO_x conversion below 35% to minimize the influence of mass and heat transfer, by following equations [1].

$$k = \frac{Q \cdot C}{m \cdot S_{BET}} \ln(1-\alpha) \quad (1)$$

$$\ln(k) = -\frac{E_a}{R \cdot T} + C \quad (2)$$

where R is 8.314 J mol^{-1} K^{-1}, T is the reaction temperature in K, Q refers to volumetric rate (100 mL min^{-1}), C is the concentration of NO (500 ppm), and α is NO_x conversion at different reaction temperatures.

Table S1. Chemical element composition and predicted fraction of Brønsted and Lewis acid sites[2].

Catalysts	Concentration of copper nitrate solution (mol/L)	Mole ratio		Acid sites	
		Si/Al_2	Cu/Al	Brønsted (mol/mol Al)	Lewis (mol/mol Al)
CuX-0.13	0.005	1.53	0.13	~0.74	~0.13
CuX-0.28	0.01	1.74	0.28	~0.44	~0.28
CuX-0.4	0.02	1.63	0.40	~0.30	~0.40
CuX-0.45	0.05	1.63	0.45	~0.25	~0.45
CuX-0.46	0.1	1.63	0.46	~0.24	~0.46
CuX-0.47	0.2	1.62	0.47	~0.23	~0.47

Table S2. The textural properties of all catalysts measured by Ar gas physisorption.

Catalysts	BET surface area (m^2/g)	Total pore volume (cc/g)	t-method		External surface area (m^2/g)
			Micropore volume (cc/g)	Micropore area (m^2/g)	
CuX-0.13	648.3	0.34	0.22	586.5	61.88
CuX-0.28	496.9	0.31	0.15	368.7	128.29
CuX-0.4	447.2	0.29	0.14	359.2	88.09
CuX-0.45	249.3	0.19	0.06	130.2	119.15
CuX-0.46	77.3	0.17	0.10	10.1	77.38
CuX-0.47	118.8	0.12	0.003	13.5	105.38

Table S3. Features observed in spectra of the concentration ME *Operando*/*in situ* IR experiments.

Wavenumber (cm^{-1})	Assignment	References
3743	stretching vibrations of isolated silanol groups (Si-OH)	3
3685	vibration of OH-groups bound to the EFAl species	3
3655	OH-groups bound to Cu^{2+} ($[Cu^{2+}(OH^-)]^+$)	4-6
3602-3588	Brønsted acidic bridging hydroxyls	5, 6
3332, 3182	NH_3 adsorbed on Cu^{2+}	7
3272, 1454	NH_4^+ (Brønsted acid site adsorbed NH_3)	6, 7
1950,1915 1927,1890,1887	Cu^{2+}-NO	8
1815	Cu^+-NO	6, 8
1828, 1735	$Cu^+(NO)_2$	8
1635，1541	tetrahedral framework Al related Brønsted acid sites	9
1610	Cu^{2+} adsorbed NH_3	10
1620,1453,1320	extra framework Al (EFAl) adsorbed NH_3	6, 9
1600-1650	bidentate bridging nitrate	7
1510,1520	the scissoring and wagging vibrations of amide($-NH_2$) species	4
1575	bridging nitrite	4
1520-1540	bidentate chelating nitrate	7
1490,1450,1430	the asymmetric and symmetric deformation of NH_4^+ bound to Brønsted acid sites	6
1480	monodentate nitrate	3
1300-1400	free-NO_3^- species of antisymmetric N-O stretches	3
1320,1330	bidentate nitrite	4-6
1272	$[Cu^{2+}(NH_3)_4]^{2+}$	5, 6

Table S4. Features observed in the time-resolved spectra of the concentration ME *Operando*/*in situ* UV-vis experiments.

Wavelength (nm)	Assignment	References
205	$Cu^{II}(OH)(NH_3)_x$	11, 12
224, 248,290	Z_2Cu^{II}	11, 12
680, 690	d-d transition band, NH_3-coordinated on Cu^{2+} sites	13
522	$Cu^{II}(NO)$	13
240,660	$Cu^{II}(NH_3)_x$	12
360	$[Cu_2O_2]^{2+}$ species	12
300-400	Nitrates adsorbed on Cu^{2+}	12

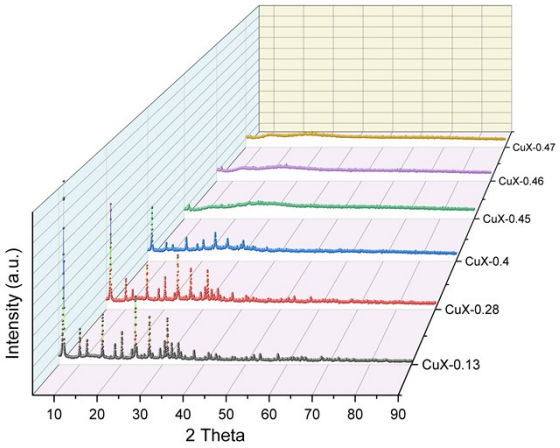

Figure S1. XRD patterns of CuX-0.13, CuX-0.28, CuX-0.4, CuX-0.45, CuX-0.46 and CuX-0.47 catalysts.

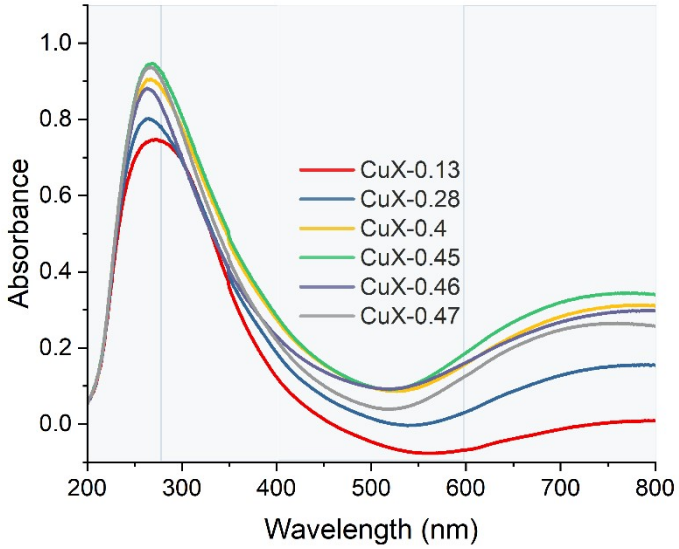

Figure S2. UV-vis spectra of the CuX-0.13, CuX-0.28, CuX-0.4, CuX-0.45, CuX-0.46 and CuX-0.47 catalysts.

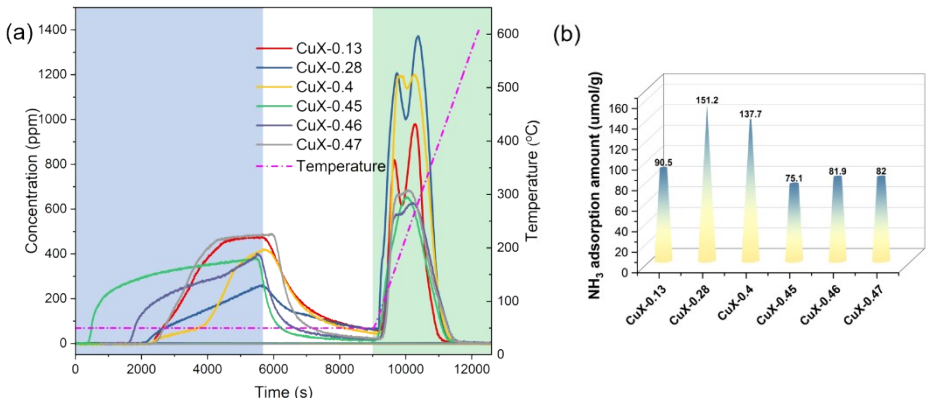

Figure S3. (a) Complete NH_3 adsorption-desorption profiles from NH_3-TPD experiments and (b) total amount of adsorbed NH_3 of CuX-0.13, CuX-0.28, CuX-0.4, CuX-0.45, CuX-0.46 and CuX-0.47.

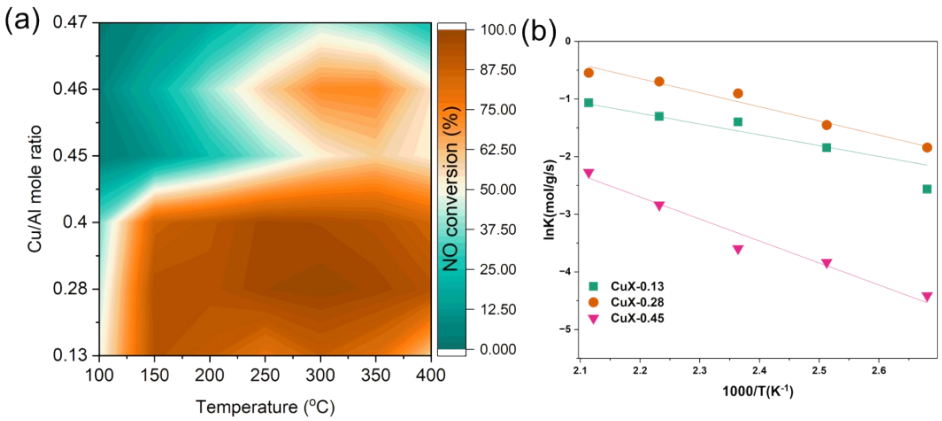

Figure S4. (a) Relationship between Cu/Al ratio and NO conversion for all catalysts; (b) Arrhenius plot for CuX-0.13, CuX-0.28, CuX-0.4, CuX-0.45.

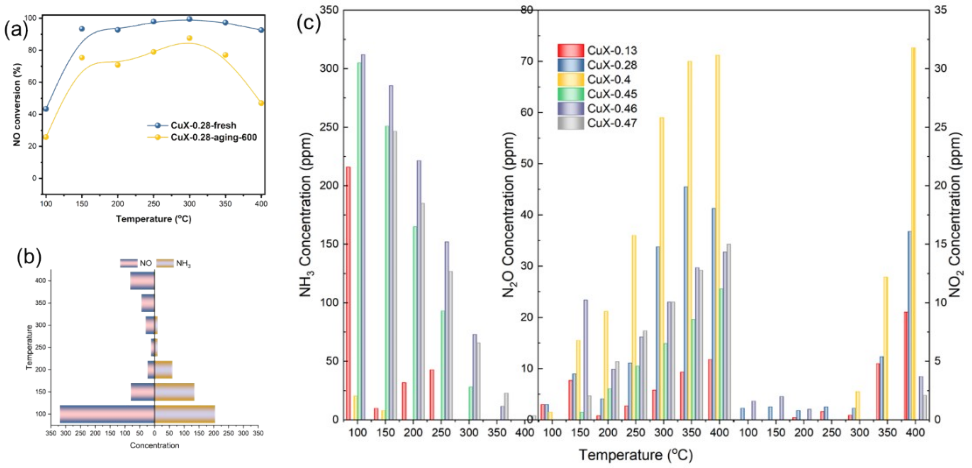

Figure S5. (a) The NO conversion of aging CuX-0.28 sample at 600°C for 8h; (b) NO and NH_3 concentration during the catalytic activity measurements of CuX-0.28 under 5% H_2O; (c) NH_3, N_2O and NO_2 concentrations obtained during the catalytic activity measurements of CuX-0.13, CuX-0.28, CuX-0.4, CuX-0.45, CuX-0.46, CuX-0.47.

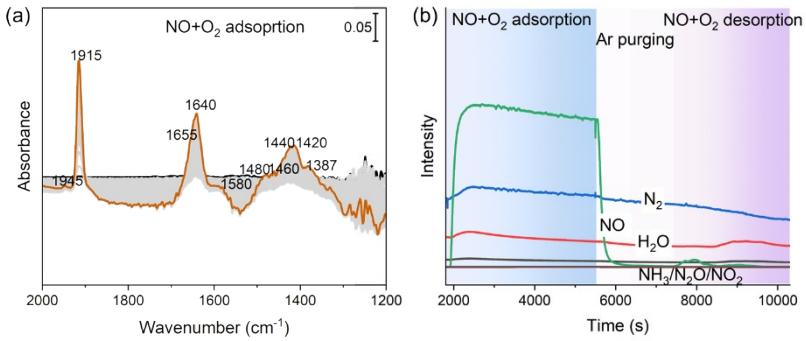

Figure S6. (a) *In situ* DRIFT spectra of CuX-0.28 during exposure to $NO+O_2$ for 60 min at 50 °C and (b) corresponding MS signals; TP = temperature programmed ramp.

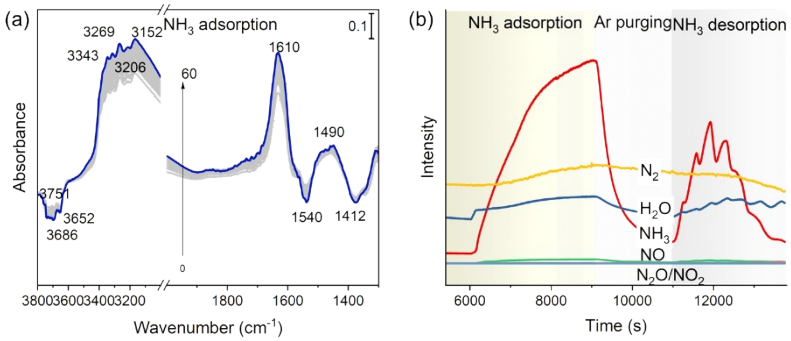

Figure S7. (a) *In situ* DRIFT spectra of CuX-0.28 during NH_3 adsorption for 60 min at 50 ^oC and (b) corresponding MS signals; TP = temperature programmed ramp.

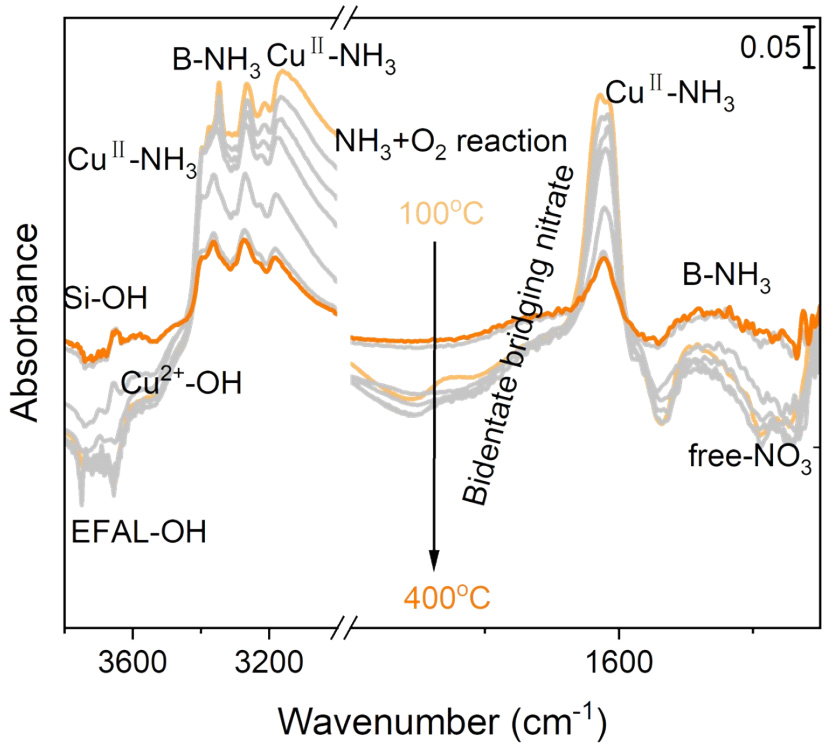

Figure S8. *In situ* DRIFT spectra of CuX-0.28 for NH_3 oxidation while heating to 400 °C

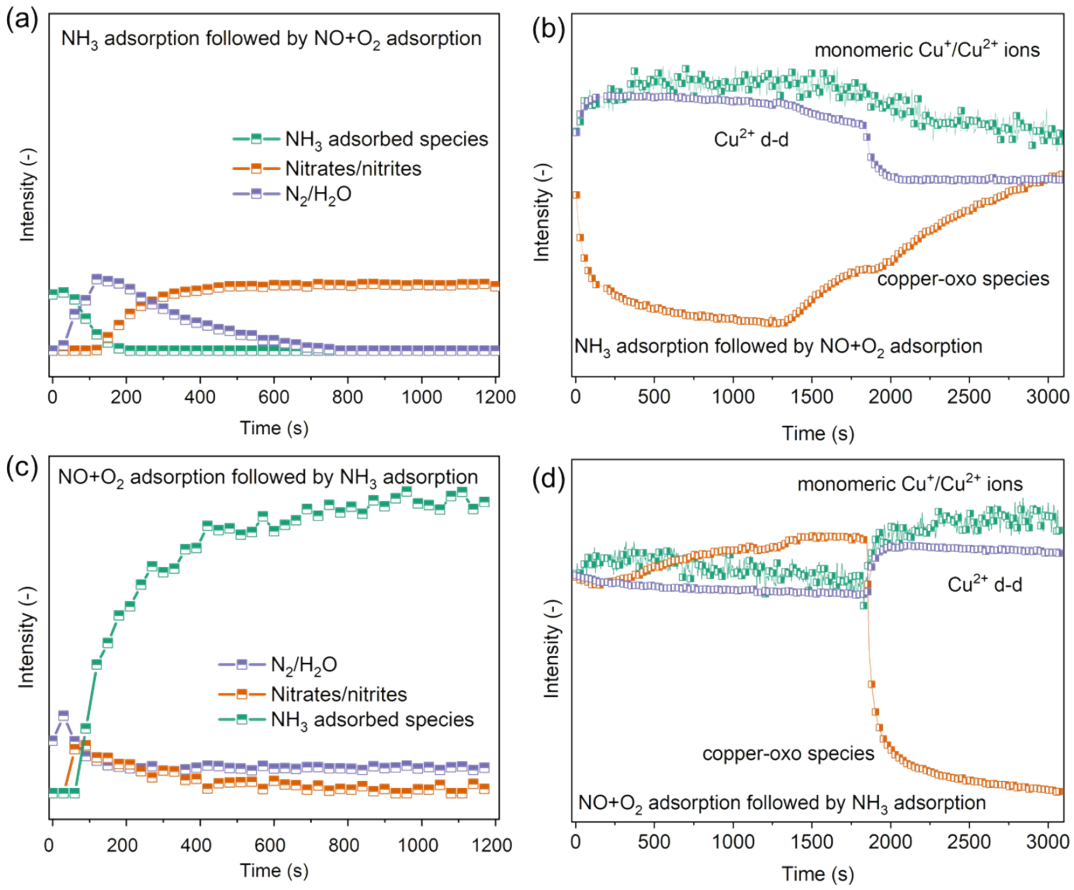

Figure S9. Corresponding time behaviors of intermediates (adsorbed NH_3 species, nitrates/nitrites and N_2/H_2O) from *in situ* DRIFT spectra under (a) NH_3 adsorption followed by $NO+O_2$ at 250 °C; (b) Exposure to $NO+O_2$ followed by NH_3 adsorption at 250 °C; (c) Time behaviors of monomeric Cu^+/Cu^{2+} ions, copper-oxo species and Cu^{2+} d-d transitions from *in situ* UV-vis spectra under (c) NH_3 adsorption followed by $NO+O_2$ at 250 °C; (d) Exposure to $NO+O_2$ followed by NH_3 adsorption at 250 °C.

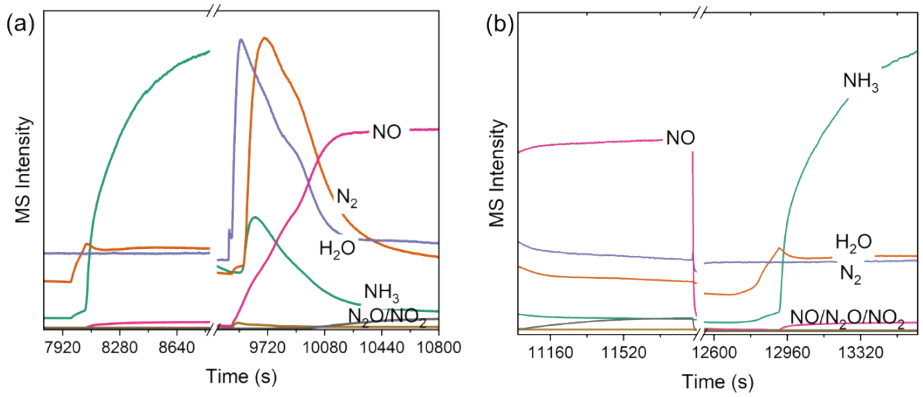

Figure S10. Evolution of MS signals during (a) NH_3 adsorption followed by $NO+O_2$ exposure at 250 ^oC over CuX-0.28 and (b) $NO+O_2$ exposure followed by NH_3 adsorption at 250 ^oC.

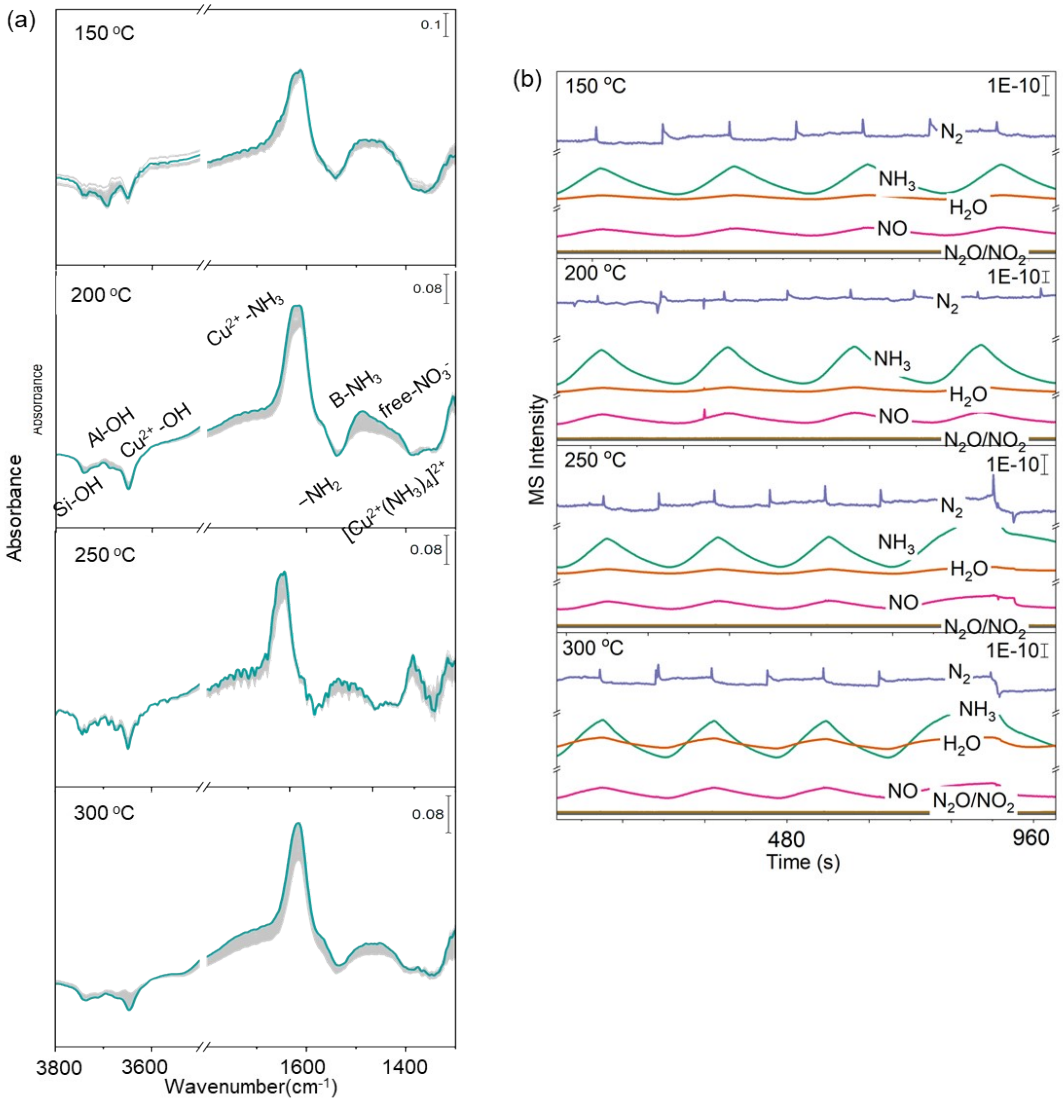

Figure S11. Time-resolved (a) DRIFT spectra of CuX-0.28 and (b) MS signals at 150, 200, 250 and 300 °C during 240 s pulses of 1000 ppm NH_3 in a gas feed of 5 vol% O_2 balanced in Ar.

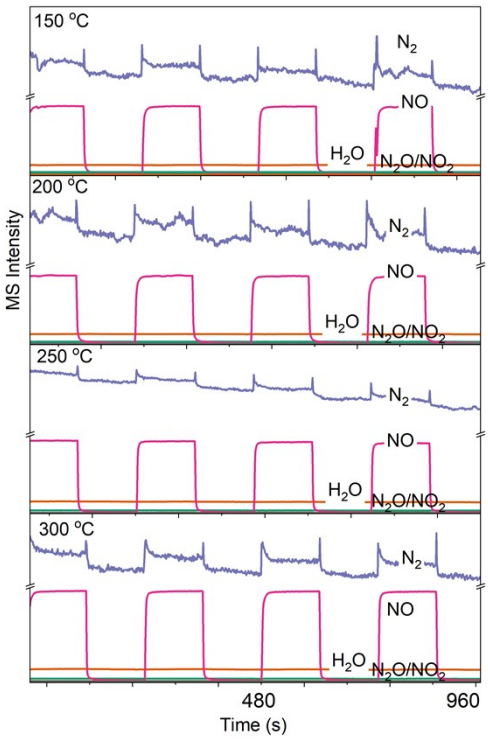

Figure S12. Evolution of MS signals at 150, 200, 250 and 300 °C during 240 s pluses of 1000 ppm NO in a gas feed of 5 vol% O_2 balanced in Ar over CuX-0.28.

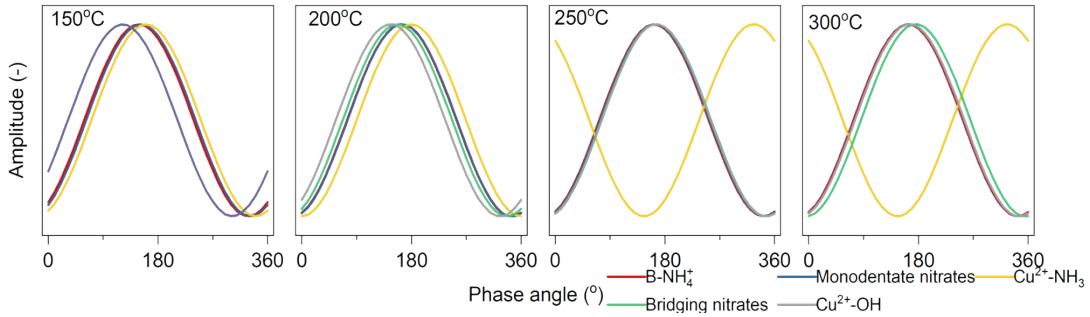

Figure S13 Normalized sinusoidal curves for the respective intermediates from *operando* DRIFT spectra (all signals are normalized between 0 and 1) at 150 °C, 200 °C, 250 °C and 300 °C during 240 s pluses of 1000 ppm NO in a gas feed of 1000 ppm NH_3 and 5 vol% O_2 in Ar.

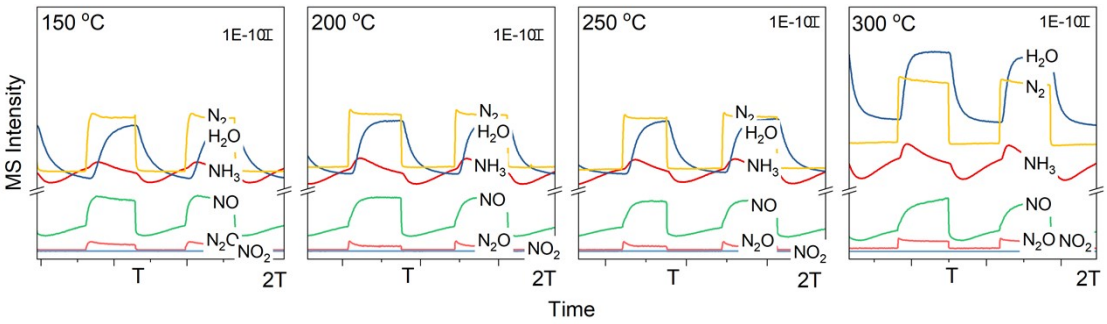

Figure S14. Evolution of MS signals at 150, 200, 250 and 300 °C during 240 s pluses of 1000 ppm NO in a gas feed of 1000 ppm NH_3 and 5 vol% O_2 balanced in Ar over CuX-0.28.

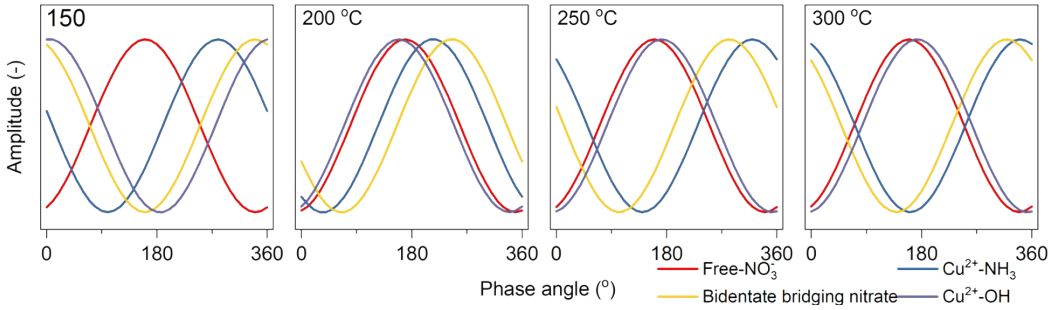

Figure S15 Normalized sinusoidal curves for the respective intermediates (all signals are normalized between 0 and 1) of *operando* ME DRIFT spectra of CuX-0.28 catalyst at 150 °C, 200 °C, 250 °C and 300 °C during 240s pluses of 1000 ppm NO or 5 vol% O_2 in a gas feed of 1000 ppm NH_3 balanced in Ar.

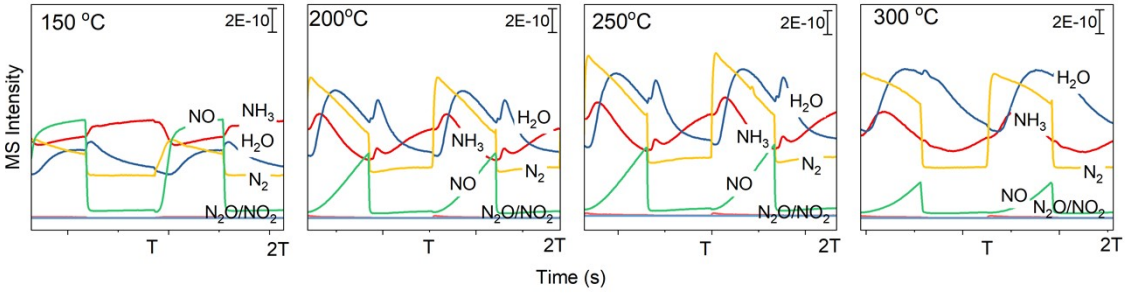

Figure S16. Evolution of MS signals at 150, 200, 250 and 300 °C during 240 s pluses of 1000 ppm NO or 5 vol% O_2 in a gas feed of 1000 ppm NH_3 balanced in Ar over CuX-0.28.

References

1. T. Zhang, T. Shi, Y. Wang, Y. Hao, Y. Gao, H. Li, L. Jia, F. Liu and S. Zeng, *J. Catal.*, 2024, **429**, 115260.
2. C. Paolucci, A. A. Parekh, I. Khurana, J. R. Di Iorio, H. Li, J. D. Albarracin Caballero, A. J. Shih, T. Anggara, W. N. Delgass, J. T. Miller, F. H. Ribeiro, R. Gounder and W. F. Schneider, *J. Am. Chem. Soc.*, 2016, **138**, 6028-6048.
3. F. Lónyi, J. Valyon and G. Pál-Borbély, *Micropor. Mesopor. Mat.* 2003, **66**, 273-282.
4. H. Wang, J. Jia, S. Liu, H. Chen, Y. Wei, Z. Wang, L. Zheng, Z. Wang and R. Zhang, *Environ. Sci. Technol.*, 2021, **55**, 5422-5434.
5. C. Negri, P. S. Hammershoi, T. V. W. Janssens, P. Beato, G. Berlier and S. Bordiga, *Chemistry*, 2018, **24**, 12044-12053.
6. A. G. Greenaway, A. Marberger, A. Thetford, I. Lezcano-Gonzalez, M. Agote-Aran, M. Nachtegaal, D. Ferri, O. Krocher, C. R. A. Catlow and A. M. Beale, *Chem. Sci.*, 2020, **11**, 447-455.
7. J. Abdul Nasir, J. Guan, T. W. Keal, A. W. Desmoutier, Y. Lu, A. M. Beale, C. R. A. Catlow and A. A. Sokol, *J. Am. Chem. Soc.*, 2023, **145**, 247-259.
8. P. Xiao, Y. Wang, Y. Lu, T. De Baerdemaeker, A.-N. Parvulescu, U. Müller, D. De Vos, X. Meng, F.-S. Xiao, W. Zhang, B. Marler, U. Kolb, H. Gies and T. Yokoi, *Appl. Catal. B: Environ. Energy*, 2023, **325**, 122395.
9. B. Tang, S. Li, W.-C. Song, E.-C. Yang, X.-J. Zhao, N. Guan and L. Li, *ACS Sustainable Chem. Eng.*, 2019, **7**, 16329-16343.
10. I. Lezcano-Gonzalez, U. Deka, B. Arstad, A. Van Yperen-De Deyne, K. Hemelsoet, M. Waroquier, V. Van Speybroeck, B. M. Weckhuysen and A. M. Beale, *Phys. Chem. Chem. Phys.*, 2014, **16**, 1639-1650.
11. A. Oda, H. Shionoya, Y. Hotta, T. Takewaki, K. Sawabe and A. Satsuma, *ACS Cataly.*, 2020, **10**, 12333-12339.
12. Y. Zhang, J. Zhang, H. Wang, W. Yang, C. Wang, Y. Peng, J. Chen, J. Li and F. Gao, *J. Phys. Chem. C*, 2022, **126**, 8720-8733.
13. A. Guo, K. Xie, H. Lei, V. Rizzotto, L. Chen, M. Fu, P. Chen, Y. Peng, D. Ye and U. Simon, *Environ. Sci. Techno.l*, 2021, **55**, 12619-12629.